THE JOURNAL OF PHYSICAL CHEMISTRY C

Article

pubs.acs.org/JPCC

Modeling Solvent Influence on Growth Mechanism of Nanoparticles (Au, Co) Synthesized by Surfactant Free Laser Processes

Paul Boyer and Michel Meunier*

Département de Génie Physique, Laser Processing and Plasmonic Laboratory, École Polytechnique de Montréal, Case Postale 6079, Succursale Centre-Ville, Montréal, Québec H3C 3A7, Canada

Supporting Information

ABSTRACT: Co and Au nanoparticles have been synthesized by femtosecond laser ablation and fragmentation in various liquids (toluene, 2-propanol, acetone, and methanol) to investigate their influences on the size of the generated particles. Results suggest that nanoparticle growth with the absence of surfactants occurs from light absorption by the colloids through diffusion coalescence and can be controlled by the solvent polarity, the processing time, and the laser power. Furthermore, the growth has been related to the electrostatic repulsion energy and to the change in the nanoparticle temperature due to the laser light absorption by using the DLVO theory. Nanosecond laser annealing of Au particles in methanol also confirms the proposed model.

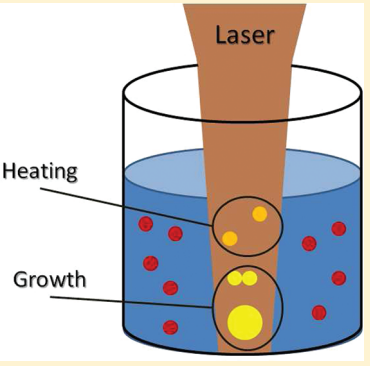

INTRODUCTION

The synthesis of nanoparticles (NPs) by laser ablation[1,2] and/or fragmentation[1−3] in liquids has been recently investigated as a one- or two-step versatile process which allows to produce NPs of any materials,[1] thus making it a useful tool for NPs development and research. It is also known as a green process[1,3,4] since it does not require the use of strong reducing agents, chemical precursors, or washing and purifying steps as used in chemical synthesis. The purity of the produced NPs and of the colloidal solution is therefore higher yielding to an expected reduced cytotoxicity and surface contamination for biomedical applications[4−6] and to a higher magnetization for ferromagnetic materials.

Solvents have a tremendous effect on the resulting NPs size and properties. The forces between charged colloids acting through a liquid medium are well-known and explained by the DLVO theory[7] that combines the effect of attraction through the van der Waals forces and an electrostatic repulsion due to electrolytes in solution. These charged ions are attracted by the colloids and create an electrical double layer around them that screens the particle surface charge. NPs aggregation can then occur by collisions through Brownian motion[8] which allow to control the final agglomerate size by tuning the electrolyte (electrostatic repulsion) and surfactant (steric repulsion) concentration. However, for the synthesis of pure nanoparticles, one would like to process NPs without using salts that could contaminate the NPs (defects, impurities) or surfactants that could hinder further functionalization[9] for biomedical applications.

During laser processes, hot atoms and aggregates are ejected inside the solvent and can generate a shockwave, a plasma plume, and a cavitation bubble.[1,2] The NPs size, ranging from 2 to 100 nm, and size distribution can be controlled by tuning the laser fluence,[1,2,10] the liquid temperature,[11] and the pressure[12] or by using surfactants.[1,2] Recent studies have also shown that NPs growth can occur inside the cavitation bubble in the initial steps[13] through Ostwald ripening. Even if the synthesis mechanisms have been addressed in the literature,[1,2,14] growth remains under investigation.

Here we report on the influence of the solvent on laser synthesized NPs of Co and Au *without* using surfactants. The NPs size in solution is changing as a function of time due to laser light absorption by the particles reaching temperatures above the solvent ebullition threshold since heat deposition is highly localized. Even if Ostwald ripening is considered to be the main growth mechanism in the laser-induced cavitation bubbles, results and simulations strongly suggest that NPs agglomerate following a diffusion coalescence process. We present and reveal why different groups have obtained different results while using the same laser parameters.[10,15−18]

EXPERIMENTAL METHODS

The NPs were synthesized using a femtosecond laser (Spectra Physics, Hurricane, 120 fs, 0.9 mJ/pulse, 10 kHz, 800 nm). For the ablation, a 99.9% pure 4 mm disk bulk target of Co or Au was placed in 30 mL of liquid. The laser was then focused with a 15 cm lens 1.6 mm below the target surface to avoid nonlinear effects in the liquid and to give a better energy transfer to the target with a processing time of 4 or 60 min. For the fragmentation, the initial solution was made from ablated

Received: September 26, 2011
Revised: March 22, 2012

   dx.doi.org/10.1021/jp2092994 | J. Phys. Chem. C XXXX, XXX, XXX−XXX

NPs with a large and wide size distribution. The laser beam was then focused inside the liquid, 1 cm below the surface. The solution was stirred by degassing with argon during the process. Nanosecond laser annealing (Brillant-B, 5 ns, 532 nm, 400 mJ/pulse, 8 mm beam, 10 Hz) was done in the same way as the fragmentation but with an unfocused beam and with a degassing flow rate 5 times smaller. This was done in order to reduce the number of bubbles that could act as small lens and therefore alter the growth mechanism from annealing to fragmentation. Au was used for the nanosecond laser annealing because of its high absorption near the laser wavelength to reduce the experimental processing time since aggregation occurs in methanol at room temperature. The NPs size distributions were probed by TEM using a Jeol-2100F on NPs dried on a carbon-coated cupper grid.

RESULTS AND DISCUSSION

In an effort to gain a better understanding of the growth behavior, NPs average size were characterized by transmission electron microscopy (TEM) after short (4 min) and long (60 min) ablation time using a femtosecond laser with a laser power of 350 mW in different solvents. In each case, more than 700NPs were counted and the experiment was repeated more than three times. Figure 1 gives an example of NPs size

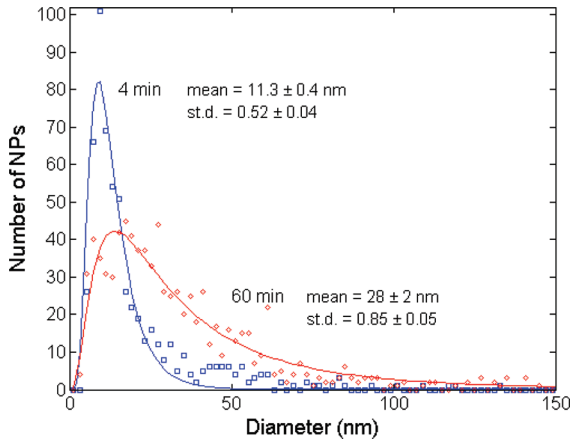

Figure 1. Histograms and log-normal fits of Co NPs ablated by a femtosecond laser in methanol at 350 mW for 4 and 60 min. The parameters "mean" and "st.d." are respectively the mean and the standard deviation that are used to characterize the log-normal distribution and the error is based on 95% confident bounds determined numerically.

distribution for short and long ablation time when synthesized in methanol. Such a process is usually described by a log-normal,[4,5,11,15] and parameters are given in Figure 1. Even if laser processes are known to generate NPs with broad size distributions, the reproducibility under the same processing conditions of the mean size and the standard deviation is less than 1 nm in acetone and around 2 nm in methanol. Although no correlation has been seen between the average diameter and the solvent properties for short ablation, a clear behavior appears for long processing time. Figure 2a shows the average diameter as a function of the solvent polarity for (in ascending order): *n*-hexane, toluene, diethyl ether, 70% toluene/30% 2-propanol, acetone, 10% toluene/90% 2-propanol, 2-propanol and methanol. The same correlation was also observed for the size dispersion (not shown). Figure 2b shows that the same trend was observed after long laser fragmentation at a power of

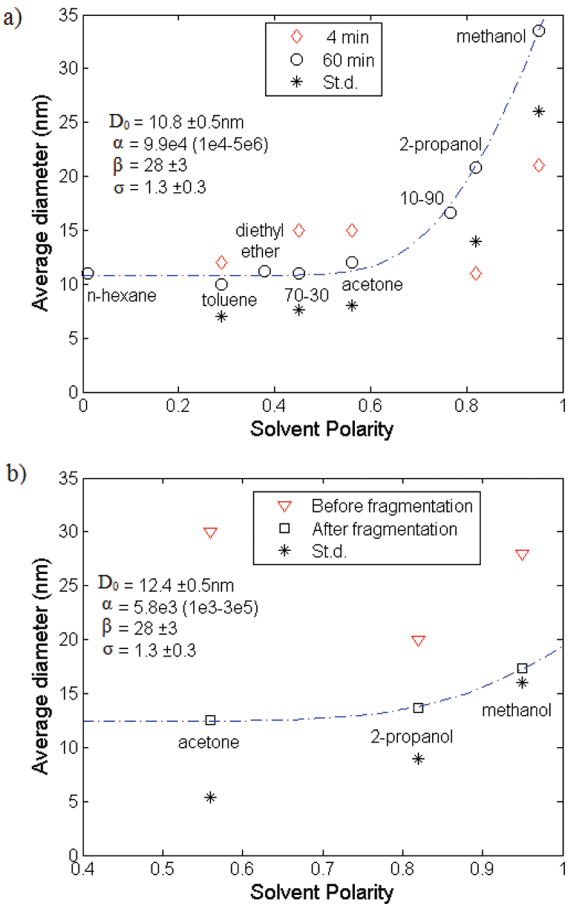

Figure 2. Average Co NPs diameter as a function of solvent polarity for (a) ablation during 4 min (diamonds) and 60 min (circles) and (b) before (triangles) and after (squares) fragmentation. The stars indicate the standard deviation after 60 min, and the error based on the reproducibility between experiments is the size of the marker used. The solutions *X*−*Y* mean *X*% toluene/*Y*% 2-propanol. The parameters D_0, α, β, and σ were obtained using eq 11 and fitting the points for (a) long ablation and (b) after fragmentation.

650 mW. Although toluene decomposition is known to generate a carbon coating, degassing with compressed air instead of argon or nitrogen during the process leads to carbon free NPs (not shown here). Degassing with compressed air was therefore used in our toluene experiments in order to avoid NPs growth quenching by the presence of the carbon matrix. Some of these solvents have also been found in the literature[19−21] to decompose and generate molecules that could act as surfactants and quench the NPs growth. In that case, laser fragmentation experiments in these solvents should have led to the formation of smaller NPs as the processing time increased due to the increase of these solvents related surfactants. Since in our experiments there was no significant change of the mean NPs size between fragmentations during 30 and 60 min, we conclude that surfactant−solvent quenching did not occur either because these surfactants were in a too small concentration or because they did not interact with the NPs or prevented coalescence.

As the ablation time increases, the NPs in solution absorb and diffuse the laser beam, leaving less energy reaching the bulk target, thus resulting in smaller produced NPs.[11] This effect can be seen in Figure 2a for small polarities, while for larger ones a growth is observed. Since the produced NPs did not show any

dx.doi.org/10.1021/jp2092994 | J. Phys. Chem. C XXXX, XXX, XXX−XXX

significant change after 2 weeks, growth is expected to occur during the laser process. Figure 3 shows a schematic of a

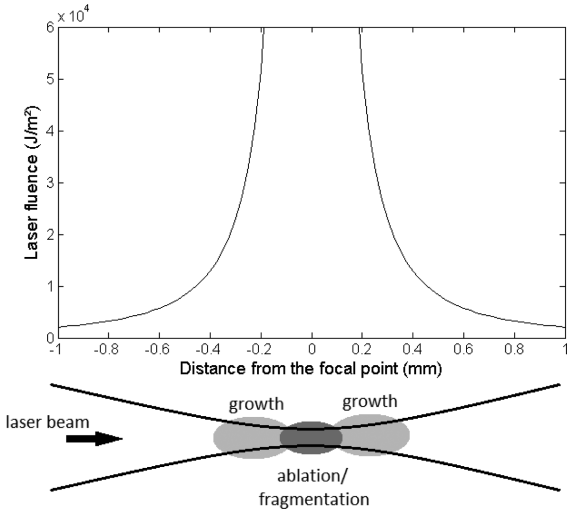

Figure 3. Laser fluence as a function of the distance from the focal point. Along the beam path, growth could occur before the ablation region. For fragmentation, growth could occur before or after the processing region at the focal point.

focused beam into a liquid where NPs are randomly distributed due to Brownian motion, sometime into the beam path and most of the time outside the beam where the NPs are probably not affected because they do not have enough kinetic energy to overcome the electrostatic repulsion from their charged surface[1,22] or to merge together. As seen in the figure, the laser fluence is expected to be high enough at the focal point to result in NPs fragmentation or ablation, while outside this zone, but still in the laser path, photon absorption yields to a heating process and growth of NPs. Growth by NPs diffusion coalescence therefore occurs in the vicinity of the focal point due to heating. Since the NPs absorption changes with the wavelength, growth could also be favored or hindered by selecting a laser wavelength at which NPs absorb respectively more or less light. Figure 1 shows that the size distribution of NPs is log-normal with a large tail to the right as is expected from diffusion coalescence growth while a left tail would have been expected for Ostwald ripening.[23] The later would imply that growth occurred through interparticle transport of single atoms, but for laser processes in liquids at a repetition rate of 1 kHz (1 ms between each pulse), the NPs are heated and cooled down rapidly[24] (around 30 ns), and they would therefore not have enough time to exchange enough atoms with their neighbors to alter significantly their size. Moreover, if this type of exchange would occur locally, the size distribution would not change much since every NP would give atoms when heated and take atoms when cooled down. If the atom exchange occurs on a larger scale, the very large NPs observed in Figure 1 could not occur by Ostwald ripening since each NP would receive very few atoms because of the dispersion. Since the NPs are hot only for a very short period of time, the only way they have of generating large particles is through the merging of NPs. Growth is therefore expected to occur through a diffusion coalescence model which is known in the limit of many coalescence events to generate a log-normal size distribution[23,25] and to increase the size dispersion. When NPs are heated by light absorption,[24] their mean free path (Brownian motion) and therefore their kinetic energy will also be increased since the surrounding solvent will also be heated but at a lower temperature. These NPs will therefore have more energy to overcome the electrostatic repulsive force and will collide together more frequently, inducing growth. The larger NPs become more stable since their mean free path varies inversely with their size. The NPs temperature increase will also allow them to increase their bounding efficiency since it will increase the diffusion of atoms to allow reshaping in order to minimize their surface tension.

We can model the growth behavior by using the perikinetic agglomeration theory[7,26,27] where the kinetic collision constant (k_a) between two particles of same size is written as

$$k_a = \frac{8k_BT}{3\mu}\exp(-V_{int}/k_BT) = k_0\exp(-V_{int}/k_BT) \quad (1)$$

where V_{int} is the maximum of the sum of the electrostatic repulsion potential (V_r) and the attractive potential (V_a, generally from the van der Waals forces) between two NPs, k_B is the Boltzmann constant, T is the NP temperature, μ is the liquid dynamic viscosity, and k_0 is the Brownian kinetic collision constant. Since the NPs have a broad size distribution with a high percentage of NPs near the mean value, we can have a good estimate of the behavior by expressing the change of the NPs concentration as a function of the NPs mean radius as

$$\frac{\partial N}{\partial t} = -k_aN^2\gamma\chi \quad (2)$$

where N is the NPs concentration, t is the growth time, γ is the binding efficiency upon collision, and χ is the volume fraction in which growth will occur. As previously shown, growth will occur in the vicinity of the focal point where the NP and the solvent temperature are high enough to overcome the electrostatic repulsion force and to induce NP reshaping and binding. By assuming that k_a and γ are almost constant, which is valid when the NPs size does not change too much, solving eq 2 yields

$$N = \frac{N_0}{1 + \gamma\chi N_0k_at} \quad (3)$$

where N_0 is the initial concentration. Since the number of nanoparticle (n) is related to the concentration by the solvent volume (V_L) and the total volume of NPs (V_{NP}) by

$$n = NV_L = \frac{V_{NP}}{(4/3)\pi R^3} \quad (4)$$

we can therefore express the change of the mean NP radius (R) as

$$R = R_0[1 + \gamma\chi N_0k_at]^{1/3} \quad (5)$$

From the DLVO theory,[7] we know that V_r between two charged spherical NPs with a low surface potential can be expressed by

$$V_r = 2\pi\varepsilon R\psi^2\exp(-\delta h) = V_{r,\infty}\exp(-\delta h) \quad (6)$$

where ε is the permittivity, ψ is the NP surface potential, $1/\delta$ is the electrical double-layer thickness, and h is the NPs

dx.doi.org/10.1021/jp2092994 | J. Phys. Chem. C XXXX, XXX, XXX–XXX

separation. We can then obtain the solution of the growth model by combining eqs 1, 5, and 6:

$$R = R_0 \left[1 + \gamma\varphi N_0 \frac{8k_B T}{3\mu} t \exp\left(\frac{-V_a - 2\pi\varepsilon R_0 \psi^2 \exp(-\delta h_{max})}{k_B T}\right)\right]^{1/3} \quad (7)$$

Since there are no electrolytes in solution, the electrostatic repulsion potential is larger than the attractive one. The maxima of the total NP potential interaction (h_{max}) will therefore be near the NP surface. Also, the double-layer thickness[27] ($1/\delta$) will become large in the absence of electrolytes since δ is proportional to the electrical charge inside the solution that screens the surface potential:

$$\delta = ze\sqrt{\frac{2cN_A}{\varepsilon k_B T}} \quad (8)$$

where N_A is Avogadro's number, c is the electrolyte concentration, e is the electronic charge, and z is the electrolyte charge. Nevertheless, δ will not be equal to zero because the solvent will induce electrical screening through its polarity (P) with less efficiency but still linearly ($\delta h_{max} \equiv P\sigma$) since a polar molecule can be oriented inside an electrical field (here from the NP); it can be attracted by its strong field gradient near the surface and plays the same electrical screening role as that of an electrolyte. σ would therefore be expressed as

$$\sigma = \eta e\sqrt{\frac{2cN_A}{\varepsilon k_B T}} h_{max} \quad (9)$$

where η would be the conversion factor to express the polarity as an effective electrolyte charge: $z = \eta P$. We can rewrite eq 7 as

$$R = R_0 \left\{1 + \left[\gamma\chi N_0 \frac{8k_B T}{3\mu} t \exp\left(\frac{-V_a}{k_B T}\right)\right] \exp\left(\frac{-V_{r,\infty} \exp(-P\sigma)}{k_B T}\right)\right\}^{1/3} \quad (10)$$

from which, by grouping factors, the change in diameter can be expressed as

$$D = D_0[1 + \alpha \exp(-\beta \exp(-p\sigma))]^{1/3} \quad (11)$$

This equation was used to fit the experimental values of Figure 2. Although the values of α, β, and σ are correlated when looking at eq 11, their allowed range of values are fixed by the constants leaving only unknown T and $\gamma\chi$ in α and T and ψ in β. We assumed that the values of σ and β were the same in both cases since the samples have the same properties (zeta potential, concentration, volume), and therefore a similar heat increase is expected in the growth region. The standard deviation of the distribution also increases when NPs grow as a result of both the initial size dispersion and the increase originating from the random collisions of the diffusion coalescence model. The values of α for ablation (9.9×10^4) and fragmentation (5.8×10^3) processes differ because in ablation new NPs are generated while in fragmentation NPs are continuously broken down. The NPs must therefore constantly restart their growth from the moment they are fragmented and not from the start of the process. Although the processing time has been strongly reduced, the change in geometry allows growth to occur above and below the focal region, leading to a doubling of the growth volume. Overall, the fragmented NPs have less time to grow which is seen by the smaller α value. The values of α, β, and σ can be found experimentally, but it is difficult to predict them since the exact values of key parameters like NP maximal temperature and ionization cannot be measured easily.

However, we can use approximated values based on the literature in order to evaluate the validity of the fit from eq 11. The solvent parameters for acetone to methanol are known: viscosity ranges from 3.06×10^{-4} to 5.44×10^{-4} m^2/s and the permittivity from 20 to 30. The time[24,28] during which the NPs are hot goes from 25 to 70 ns depending upon the liquid heat conductivity and the laser deposited energy. Since the thermal conductivity of liquids is much smaller than the one for the NPs, the solvent heating is localized in the vicinity of the NPs in the growth region. In addition, the shockwave also increases the solution kinetic energy leading to an effective temperature increase of the solvent. Both these effects will locally heat the solvent and its temperature is estimated to be between 300 and 500 K. Mafuné et al.[29] have seen that the charge state for nanosecond laser fragmentation could be increased from 60 to more than 710. Although we cannot measure it directly, the NPs in the growth region after the femtosecond laser pulse could have a charged state around 120 mV for a short period of time after the laser pulse based on results from Mafuné.[29] Assuming that the initial NPs radius is of 6 nm (from Figure 2), that the ablated mass is of 3.65×10^{-4} g, that the growth volume is of 1 mm^3, and that the other parameters are taken to be the average of the expected values, we obtain the following values for eq 11: $\alpha = 3.9 \times 10^5$ and $\beta = 26$. Therefore, using literature values, we obtained values that are near the ones obtained by the fit of eq 11 on the results from Figure 2a which confirms the idea that growth occurred through a diffusion coalescence process.

In order to see if the growth occurs from light absorption by the NPs or from the heat released by the ablation or the fragmentation, we have performed nanosecond laser annealing at 532 nm for 30 min at 10 Hz in methanol with an unfocused beam on Au NPs that were previously synthesized by laser fragmentation. Using the equations from Letfullin et al.,[24] we have modeled the estimated average temperature increase of 35 nm Au nanoparticles for laser powers of 30, 70, and 200 mW by solving

$$C(T)\rho\frac{\partial T}{\partial t} = \frac{3K_{abs}I_0 f(t)}{4R_0} - \frac{\mu_\infty T}{(s+1)R_0{}^2}\left[\left(\frac{T}{T_\infty}\right)^{s+1} - 1\right] \quad (12)$$

where K_{abs}, I_0, $f(t)$, C, T_∞, ρ, μ_∞, and s are respectively NP absorption efficiency (4.02 from the Mie theory[30]), laser intensity, laser time profile (5 ns Gaussian), specific heat (129 J/(K kg)), solvent temperature (298 K), NP density (0.0193 kg/cm^3), solvent heat conductivity (0.21 W/(K m) at 298 K), and a constant depending upon the thermal properties of the solvent ($s = 1$). Table 1 shows the average diameter measured by TEM as a function of the laser power and the estimated temperature as deduced from eq 12. The estimated NP maximum temperature achieved in this experiment is below the melting temperature of gold (1337 K) which supports the idea that growth does not originate from Ostwald ripening because atoms evaporation from the NP would not be significant during

dx.doi.org/10.1021/jp2092994 | J. Phys. Chem. C XXXX, XXX, XXX–XXX

Table 1. Measured Average Au NPs Diameter as a Function of the Nanosecond Laser Annealing Temperature Estimated from Laser Powers: 580 K for 30 mW, 740 K for 60 mW, and 1020 K for 200 mW

laser power (mW)	est temp (K)	average diam (nm)	std dev (nm)	mass-weighted average (nm)
0	293	32	24	49
30	580	47	33	69
70	737	51	33	74
200	1016	53	66	122

its short excited time. By analyzing the NPs size, we considered that NPs were spherical even for the 200 mW sample. This can lead to an underestimation of the size since some NPs can be partially bounded by their surface without having completely merged and were counted separately in the measurements since we could not identify them. Nevertheless, we can see that growth as occurred even at low laser powers and increases slowly as the NPs temperature becomes higher. Since the number of laser pulses is small and the degassing was 5 times smaller than for femtosecond processes, growth occurs with NPs that are in their vicinity and have less time to homogenize the size distribution through the solution which becomes very large. This can be seen in Figure 4 where large and small NPs

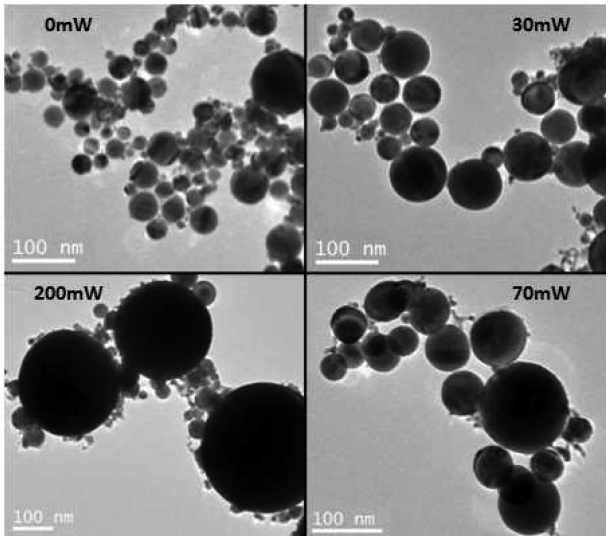

Figure 4. TEM pictures of Au NPs annealed with an unfocused nanosecond laser at 532 nm in methanol for various laser power.

can be simultaneously seen even in the sample annealed at 200 mW and in Table 1 by the difference between the average diameter and the mass weighted average diameter. The fast growth that occurred at 30 mW and the slow increase at higher laser powers cannot be explained by Ostwald ripening since an increase of the NPs temperature should have brought a faster evaporation/exchange of atoms and therefore a faster growth. The slow growth can only be explained by the diffusion coalescence model with the slow increase of the solvent temperature coming from the NPs and therefore slowly increasing NPs collisions. The initial fast growth is also consistent with the model since NP reshaping occurs only above a fix temperature although some collisions occurs a room temperature in methanol. Nevertheless, results shown in Figure 4 indicate that the collision frequency is dependent upon the laser power since an increase of the NPs size is observed. If the collision frequency was not altered by the laser, NPs growth would have be limited since the number of NPs merging together would have remain constant and therefore would not show large differences as the laser power is increased above the reshaping threshold. The formation of very big particles at higher laser power indicates that there is an increase in the number of interacting NPs, suggesting that the laser stimulated the collision frequency. Nanosecond laser annealing can therefore be used as a second processing step in order to induce NPs growth through a diffusion coalescence process. Overall, it is clear that light absorption by the NPs can lead to growth in solution during laser processes and therefore needs to be taken under consideration when fabricating NPs by laser processes.[31]

CONCLUSION

In summary, a careful choice of solvent during laser processes permits to control the NPs physical properties without having to reduce the yield by lowering the laser fluence or by using surfactants that can hinder further functionalization for biomedical applications or catalytic processes. This can be achieved by controlling growth through the liquid polarity that plays the same role as the electrolyte in the DLVO theory but with the advantage that laser allows to achieve NP temperatures above the solvent ebullition point due to localized heating of the particles which would not have been possible in chemical synthesis. The NPs size can also be altered by growth from nanosecond laser annealing. In both cases, the increase in the NPs size originated from their heating caused by the absorption of some of the laser light through a diffusion coalescence model. This allows us to have a better control of the final NPs size while keeping them pure from impurities or surface contamination.

ASSOCIATED CONTENT

Supporting Information

TEM pictures of Co NPs synthesized by laser ablation in toluene degassed with nitrogen or compressed air showing respectively the formation and the absence of a carbon matrix around the NPs. This material is available free of charge via the Internet at http://pubs.acs.org.

AUTHOR INFORMATION

Corresponding Author

*E-mail: michel.meunier@polymtl.ca.

Notes

The authors declare no competing financial interest.

ACKNOWLEDGMENTS

The authors acknowledge Yves Drolet for his technical help and the Canadian Research Chair on laser micro/nanoengineering of materials for financial contributions. P.B. also acknowledges the Natural Science and Engineering Research Council of Canada for his scholarship.

REFERENCES

(1) Amendola, V.; Meneghetti, M. Laser ablation synthesis in solution and size manipulation of noble metal nanoparticles. *Phys. Chem. Chem. Phys.* **2009**, *11*, 3805−3821.

(2) Sugioka, K.; Meunier, M.; Piqué, A. *Laser Precision Microfabrication*; Springer Series in Materials Science; Springer: Berlin, Germany, 2010.
(3) Besner, S.; Kabashin, A. V.; Meunier, M. Fragmentation of colloidal nanoparticles by femtosecond laser-induced supercontinuum generation. *Appl. Phys. Lett.* **2006**, *89*, 233122.1−3.
(4) Yang, S.; Cai, W.; Zhang, H.; Xu, X.; Zeng, H. Size and structure control of Si nanoparticles by laser ablation in different liquid media and further centrifugation classification. *J. Phys. Chem. C* **2009**, *113*, 19091−19095.
(5) Barcikowski, S.; Hahn, A.; Kabashin, A. V.; Chichkov, B. N. Properties of nanoparticles generated during femtosecond laser machining in air and water. *Appl. Phys. A: Mater. Sci. Process.* **2007**, *87*, 47−55.
(6) Besner, S.; Kabashin, A. V.; Winnik, F. M.; Meunier, M. Ultrafast laser based "green" synthesis of non-toxic nanoparticles in aqueous solutions. *Appl. Phys. A: Mater. Sci. Process.* **2008**, *93*, 955−959.
(7) Elimelech, M.; Gregory, J.; Jia, X.; Williams, R. A. *Particle Deposition and Aggregation − Measurement, Modeling and Simulation*; Butterworth-Heinemann: Woburn, MA, 1995.
(8) Hywel, M. *AC Electrokinetics: Colloids and Nanoparticle*; Research Studies Press: Hertfordshire, England, 2003.
(9) Berry, C. C. Progress in functionalization of magnetic nanoparticles for applications in biomedicine. *J. Phys. D: Appl. Phys.* **2009**, *42*, 224003.1−9.
(10) Sylvestre, J.-P.; Kabashin, A. V.; Sacher, E.; Meunier, M. Femtosecond laser ablation of gold in water: influence of the laser-produced plasma on the nanoparticle size distribution. *Appl. Phys. A: Mater. Sci. Process.* **2005**, *80*, 753−758.
(11) Menéndez-Manjón, A.; Chichkov, B. N.; Barcikowski, S. Influence of water temperature on the hydrodynamic diameter of gold nanoparticles from laser ablation. *J. Phys. Chem. C* **2010**, *114*, 2499−2504.
(12) Soliman, W.; Takada, N.; Sasaki, K. Effect of water pressure on the size of nanoparticles in liquid-phase laser ablation. *IEEE Region 10 Conf. (Tencon)* **2010**, 154−157.
(13) Soliman, W.; Takada, N.; Sasaki, K. Growth processes of nanoparticles in liquid-phase laser ablation studied by laser-light scattering. *Appl. Phys. Express* **2010**, *3*, 035201.1−3.
(14) Mafuné, F.; Kohno, J.-Y.; Takeda, Y.; Kondow, T. Structure and stability of silver nanoparticles in aqueous solution produced by laser ablation. *J. Am. Chem. Soc.* **2000**, *104*, 8333−8337.
(15) Barcikowski, S.; Menéndez-Manjón, A.; Chichkov, B. Generation of nanoparticle colloids by picoseconds and femtosecond laser ablations in liquid flow. *Appl. Phys. Lett.* **2007**, *91*, 083113.1−3.
(16) Kabashin, A.; Meunier, M. Synthesis of colloidal nanoparticles during femtosecond laser ablation of gold in water. *J. Appl. Phys.* **2003**, *94*, 7941−7943.
(17) Kim, H. J.; Bang, I. C.; Onoe, J. Characteristic stability of bare Au-water nanofluids fabricated by pulsed laser ablation in liquids. *Opt. Laser Eng.* **2009**, *47*, 532−538.
(18) Simakin, A. V.; Voronov, V. V.; Kirichenko, N. A.; Shafeev, G. A. Nanoparticles produced by laser ablation of solids in liquid environment. *Appl. Phys. A: Mater. Sci. Process.* **2004**, *79*, 1127−1132.
(19) Phuoca, T. X.; Howarda, B. H.; Martelloa, D. V.; Soonga, Y.; Chyub, M. K. Synthesis of $Mg(OH)_2$, MgO, and Mg nanoparticles using laser ablation of magnesium in water and solvents. *Opt. Laser Eng.* **2008**, *46*, 829−834.
(20) Kazakevich, P. V.; Voronov, V. V.; Simakin, A. V.; Shafeev, G. A. Production of copper and brass nanoparticles upon laser ablation in liquids. *J. Quant. Elect.* **2004**, *34*, 951.
(21) Hu, A.; Sanderson, J.; Zaidi, A. A.; Wand, C.; Zhang, T.; Zhou, Y.; Duley, W. W. Direct synthesis of polyyne molecules in acetone by dissociation using femtosecond laser irradiation. *Carbon* **2008**, *46*, 1823−1825.
(22) Sylvestre, J.-P.; Kabashin, A. V.; Sacher, E.; Meunier, M.; Luong, J. H. T. Stabilization and size control of gold nanoparticles during laser ablation in aqueous cyclodextrins. *J. Am. Chem. Soc.* **2004**, *126*, 7176−7177.
(23) Granqvist, C. G.; Buhrman, R. A. Size distributions for supported metal catalyst: coalescence growth versus Ostwald ripening. *J. Catal.* **1976**, *42*, 477−479.
(24) Letfullin, R. R.; George, T. F.; Duree, G. C. Bollinger, B.M. Ultrashort laser pulse heating of nanoparticles: comparison of theoretical approaches. *Adv. Opt. Technol.* **2008**, *251718*, 8.
(25) Grandvist, C. G.; Buhrman, R. A. Statistical model for coalescence of islands in discontinuous films. *Appl. Phys. Lett.* **1975**, *27*, 693−694.
(26) Smoluchowski, M. Versuch einer mathematischen theorie der koagulationskinetik kolloider losungen. *Z. Phys. Chem.* **1917**, *92*, 129.
(27) Rector, D. R.; Bunker, B. C. Effect of colloidal aggregation of the sedimentation and rheological properties of tank waste. *PNL-10761* **1995**, Sept 01.
(28) Hodak, J. H.; Henglein, A.; Giersig, M.; Hartland, G. V. Laser-induced inter-diffusion in AuAg core-shell nanoparticles. *J. Phys. Chem. B* **2000**, *104*, 11708−11718.
(29) Yamada, K.; Tokumoto, Y.; Nagata, T.; Mafuné, F. Mechanism of laser-induced size-reduction of gold nanoparticles as studied by nanosecond transient absorption spectroscopy. *J. Phys. Chem. B* **2006**, *110*, 11751−11756.
(30) Mie, G. Beiträge zur optic trüber medien, speziell kolloidaler metallösungen. *Ann. Phys. (Leipzig)* **1908**, *25*, 377−445.
(31) Better predictions and fitting could be achieved using the extended DLVO theory which gives a better approximation of the repulsion energy and by resolving numerically the equations for each NP (considering their different radius), especially when the size distribution becomes large. The binding efficiency as a function of temperature and the influence of surfactants as growth limiter should also be studied to gain a better control over the process.